

# Spectral Properties and Magic Generation in $T$ -doped Random Clifford Circuits

Dominik Szombathy,<sup>1,2,\*</sup> Angelo Valli,<sup>1,3</sup> Cătălin Pașcu Moca,<sup>3,4</sup>  
János Asbóth,<sup>1,5</sup> Lóránt Farkas,<sup>2</sup> Tibor Rakovszky,<sup>1,6,7</sup> and Gergely Zaránd<sup>1,3,†</sup>

<sup>1</sup>*Department of Theoretical Physics, Institute of Physics,  
Budapest University of Technology and Economics,  
Műgyetem rkp. 3., H-1111 Budapest, Hungary*

<sup>2</sup>*Nokia Bell Labs, Nokia Solutions and Networks Kft,  
1083 Budapest, Bókay János u. 36-42, Hungary*

<sup>3</sup>*MTA-BME Quantum Dynamics and Correlations Research Group,  
Budapest University of Technology and Economics,  
Műgyetem rkp. 3., H-1111 Budapest, Hungary*

<sup>4</sup>*Department of Physics, University of Oradea, 410087, Oradea, Romania*

<sup>5</sup>*HUN-REN Wigner Research Centre for Physics, H-1525 Budapest, P.O. Box 49., Hungary*

<sup>6</sup>*HUN-REN-BME Quantum Error Correcting Codes and Non-equilibrium Phases Research Group,  
Budapest University of Technology and Economics,  
Műgyetem rkp. 3., H-1111 Budapest, Hungary*

<sup>7</sup>*Department of Physics, Stanford University, Stanford, California 94305, USA*

(Dated: December 23, 2024)

We study the emergence of complexity in deep random  $N$ -qubit  $T$ -gate doped Clifford circuits, as reflected in their spectral properties and in magic generation, characterized by the stabilizer Rényi entropy. For pure (undoped) Clifford circuits, a unique periodic orbit structure in the space of Pauli strings implies peculiar spectral correlations and level statistics with large degeneracies.  $T$ -gate doping induces an exponentially fast transition to chaotic behavior, described by random matrix theory. To characterize magic generation properties of the Clifford+ $T$  ensemble, we determine the distribution of magic, as well as the average nonstabilizing power of the quantum circuit ensemble. In the dilute limit,  $N_T \ll N$ , magic generation is governed by single-qubit behavior, and magic increases linearly with the number of  $T$ -gates,  $N_T$ . For  $N_T \gg N$ , magic distribution converges to that of Haar-random unitaries, and averages to a finite magic density,  $\mu$ ,  $\lim_{N \rightarrow \infty} \langle \mu \rangle_{\text{Haar}} = 1$ . Although our numerics has large finite-size effects, finite size scaling reveals a magic density phase transition at a critical  $T$ -gate density,  $n_T^* = (N_T/N)^* \approx 2.41$  in the  $N \rightarrow \infty$  limit. This is in contrast to the spectral transition, where  $\mathcal{O}(1)$   $T$ -gates suffice to remove spectral degeneracies and to induce a transition to chaotic behavior in the thermodynamic limit. Magic is therefore a more sensitive indicator of complexity.

## I. INTRODUCTION

Quantum physics has opened up a complexity frontier: generic quantum dynamics can easily turn a product state of many particles or qubits into a state that is practically impossible to represent, let alone study, on a classical computer [1]. A possible source of complexity is quantum entanglement [2] generated between the constituents; without this, quantum dynamics is efficiently simulable classically [3, 4]. However, entanglement in itself does not fully characterize this frontier, as there exist dynamics that create highly entangled states and yet can be efficiently simulated classically. A chief example is that of Clifford circuits, which have an efficient representation in terms of the so-called stabilizer formalism [5, 6], while they generate entanglement [7, 8]. For these properties, Clifford circuits are often used as easily simulable toy models of quantum many-body dynamics, where various quantities of interest can be studied numerically [7, 9, 10].

While Clifford circuits exhibit certain properties similar to generic quantum dynamical systems, their efficient simulability comes with some highly non-generic qualities [11]. They are generally considered to lack complexity, a property closely tied to the notion of “*nonstabilizerness*” or “*magic*” [12]. States that cannot be generated by Clifford circuits from computational basis states exhibit a quantum resource referred to as magic. Such states are not efficiently representable using the stabilizer formalism and serve as valuable resources for producing generic states [13]. The simplicity or the complexity of a *circuit* can therefore be assessed by examining the magic of the states it produces from basis states, referred to as the *nonstabilizing power* of the circuit [12]. A circuit can be considered insufficiently complex if the resulting states exhibit low magic. The concept of magic, which quantifies aspects of quantumness and non-simulability, has been extensively studied in recent years and can be measured using various methods [12, 14–28].

Another possible tool to assess the lack of complexity of a circuit is provided by *spectral correlations*. As we demonstrate in this work, the spectral properties of Clifford circuits are very peculiar: the spectrum does not display level repulsion, characteristic to chaotic systems

\* szombathy.dominik@edu.bme.hu

† zarand.gergely.attila@ttk.bme.hu

or Haar-random circuits, although it is neither Poissonian.

It has been known for a longtime that extended “Clifford+ $T$ -gate sets” realize a platform for universal quantum computation, and can therefore be used to approximate arbitrary unitary operations [29]. The realization of  $T$ -gates is thus an important task for fault-tolerant quantum computation, where this is often done using magic states and gate teleportation, and often consumes much of the resources of a computation [16, 26, 30]. Interestingly, while adding a small number of  $T$ -gates does not spoil classical simulability [31], it is already sufficient to make a quantum circuit mimic a generic unitary ensemble [32], and even a single  $T$ -gate in a Clifford circuit can drive a transition to universal entanglement spectrum statistics [33].

In this work, we address the question, how introducing  $T$ -gates into Clifford circuits induces complexity by the above measures. Instead of limiting ourselves to specific examples, we consider an ensemble of random Clifford circuits and study its statistical properties to uncover typical behavior, while focusing on two different but complementary aspects: (i) the structure and evolution of the peculiar Clifford spectrum, and (ii) the way magic is generated by injected  $T$ -gates. We find that nonstabilizerness and spectral correlations of random Clifford circuits reveal increasing complexity upon “doping” with  $T$ -gates.

First, to uncover spectral properties of pure Clifford circuits with no  $T$ -gates, we relate spectral correlations to the distribution of periodic orbits in the space of Pauli strings. Dynamics there decomposes into periodic orbits, giving rise to a peculiar “Clifford spectrum”, which exhibits large degeneracies, while it is clearly distinct from a Poissonian spectrum usually associated with integrable systems. Introducing  $T$ -gates disrupts these orbits, the peculiar Clifford spectrum gradually disappears, and evolves into a generic chaotic behavior described by random-matrix theory (RMT), as signalled by various indicators. Our results suggest that an  $\mathcal{O}(1)$  number of  $T$ -gates suffices to make the average spectral properties RMT-like, resembling the scaling observed for other measures of chaos [32, 33]. This behavior is somewhat analogous to the property of perturbed classical integrable systems, where – according to the KAM theorem [34] – a small nonintegrable perturbation cannot entirely destroy periodic orbits in the entire phase space.

To understand how magic is generated, we rely on a particular magic quantifier, the recently introduced (second) *stabilizer Renyi entropy* (SRE) [12, 35, 36],  $M_2$ , also referred to as magic. However, instead of focusing on the magic contained in a state, we concentrate on characterizing the magic (generation) properties of specific *ensembles of quantum operations* [37, 38]. By a statistical sampling of deep Clifford+ $T$  circuits, we obtain the corresponding SRE (magic) distribution and investigate its evolution as a function of the number of injected  $T$ -gates,  $N_T$ . Averaging also allows us to compute the average nonstabilizing power of the circuit ensemble,  $\langle \mathcal{M}_2 \rangle$ .

We find that, in the dilute limit,  $N_T \ll N$ , where  $N$  is the number of qubits, magic is typically generated in discrete steps (quanta), and the average nonstabilizing power increases linearly with the number of  $T$ -gates in large circuits. For an extensive number of injected  $T$ -gates, a continuum of SRE distribution emerges, which eventually converges to that of the Haar random unitary ensemble. In the thermodynamic limit,  $N \rightarrow \infty$ , a phase transition emerges: above a critical density of  $T$ -gates,  $n_T^* \equiv (N_T/N)^* \approx 2.41$ , the average magic density  $\langle M_2/N \rangle = \langle \mathcal{M}_2/N \rangle$  generated by the circuit approaches its maximal value,  $\langle M_2/N \rangle \rightarrow 1$ , while below this critical density magic density is just proportional to  $n_T$ . These findings are in line with the observation that certain features of *stabilizerness require a finite density* of  $T$  gates to disappear [39].

The manuscript is organized as follows. In Sec. II we discuss the anatomy of the random circuits considered in this work. Section III is devoted to the analysis of the spectral properties. In Sec. III A we recall the relevant notions of Clifford algebra to derive the peculiar structure of the periodic orbits and its relation to the eigenvalue spectrum, whereas in Sec. III B we discuss the effects of injecting  $T$ -gates on the the eigenvalue correlation function and the level spacing statistics. Sec. IV focuses on magic. We start from the paradigmatic case of a single qubit in Sec. IV B, which holds the key to understand the magic generation mechanism Clifford+ $T$  circuits, as discussed in Sec. IV C. Finally, Sec. V contains our conclusion and an outlook.

## II. T-DOPED RANDOM CLIFFORD CIRCUITS

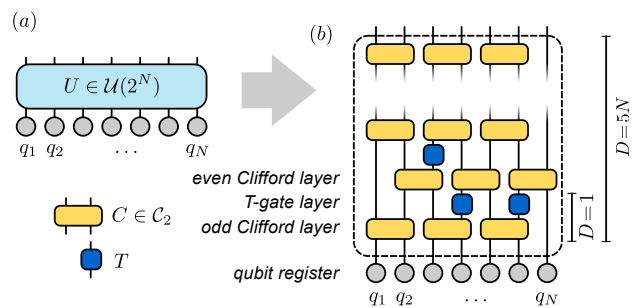


FIG. 1. (a) Unitary operator  $U \in \mathcal{U}(2^N)$  operating on a  $N$ -qubit register  $\{q_1, q_2, \dots, q_N\}$ . (b) Schematic construction of a brick-wall random Clifford+ $T$  gates circuit. Each layer includes 2-qubit Clifford gates  $C \in \mathcal{C}_2$  acting on neighboring qubits and (for doped circuits) a layer of randomly injected  $T$ -gates. Typical circuits considered in the following contain  $D = 5N$  such layers (see text for details).

Let us start by characterizing the class of random circuits under consideration, schematically represented in Fig. 1. Given an array of  $N$  qubits, we build circuits with a *brick-wall* structure, i.e., composed of odd and

even layers of 2-qubit Clifford gates  $C \in \mathcal{C}_2$ . Each gate is chosen randomly with uniform probability from all possible  $|\mathcal{C}_2| = 11520$  2-qubit Clifford gates. The depth  $D$  of a circuit is given by the number of layers. Additionally, after each Clifford layer, we include another layer in which we inject  $T$ -gates ( $\pi/4$  phase gates). For a given total number  $N_T$  of  $T$ -gates in the circuit, both the layer index  $l$  and the qubit index  $i$  on which the  $T$ -gate acts are chosen randomly, with a constraint preventing  $T$ -gates to have the same  $(l, i)$  pair, since the action of two consecutive  $T$ -gates corresponds to a phase gate  $T^2 = S$ , which belongs to the Clifford group.

We note that the particular choice of brick-wall architecture is largely unimportant for our discussion below. We will be interested in the limit of deep circuits,  $D \gg N$ , and in this limit the random brick-wall Clifford-circuit ensemble becomes indistinguishable from the uniform distribution over *all*  $N$ -qubit Clifford unitaries. Therefore, the results that we obtain for (deep) brick-wall construction are representative of the Clifford group  $\mathcal{C}_N$ . The necessary depth  $D$  needed to achieve this limit is related to entanglement spreading. In particular, we expect a linear growth of entanglement, characterized by an “entanglement velocity” [40, 41], which sets the number of layers needed to entangle all qubits; this required depth is therefore expected to scale linearly with the system size  $N$ . We verified numerically that the spectral properties of the Clifford circuits converge with respect to the circuit depth.

The choice of the brick-wall structure provides a number of advantages. In particular, it is computationally efficient to (i) build and apply the *tableau* determining the action of each 2-qubit Clifford gates on strings, and (ii) to sample a collection of 2-qubit gates rather than a single  $N$ -qubit gate, since such operation scales with  $\mathcal{O}(N^2)$  for state-of-the-art algorithms [42, 43].

### III. SPECTRAL PROPERTIES OF DOPED CLIFFORD CIRCUITS

Our goal is to characterize the spectral properties of random  $T$ -doped brick-wall Clifford circuits (henceforth Clifford circuits). Before turning to the  $T$ -doped case, let us investigate the rather peculiar spectral properties of undoped Clifford circuits.

#### A. Spectral properties of pure Clifford circuits

An  $N$ -qubit Clifford operator  $C$  acts on the  $2^N$  dimensional Hilbert space of the  $N$  qubits. A Clifford operator takes Pauli strings  $S$  to Pauli strings via conjugation (up to a global phase),  $S \rightarrow C S C^\dagger$ . More formally, the Clifford group  $\mathcal{C}_N$  acting on a  $N$ -qubit register is defined as

$$\mathcal{C}_N = \left\{ C \in \mathcal{U}(2^N) \mid C \tilde{\mathcal{P}}_N C^\dagger = \mathcal{P}_N \right\} / \mathcal{U}(1) \quad (1)$$

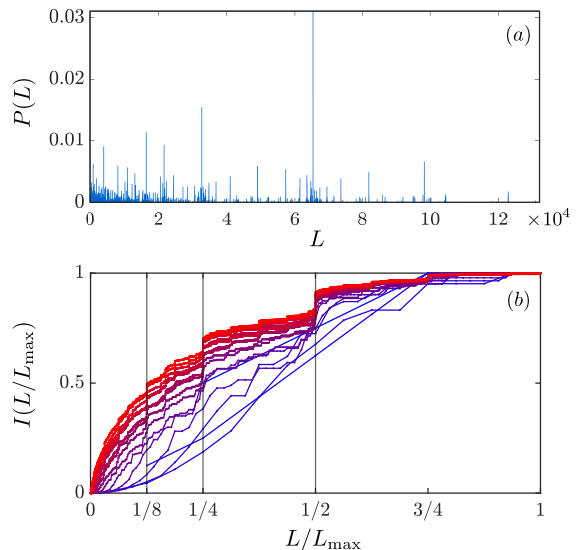


FIG. 2. (a) Parity-integrated probability  $P(L)$  for  $N = 16$ . (b) Integrated probabilities  $I(L/L_{\max})$  for  $N = \{2, 3, \dots, 16\}$  (from blue to red). The vertical black lines denote representative rational values  $L/L_{\max} = p/q$ .

where  $\mathcal{P}_N$  denotes the set of *unsigned*  $N$ -qubit Pauli strings, whose elements are generated by the tensor product of single-qubit signed Pauli matrices, and  $\tilde{\mathcal{P}}_N = \mathcal{P}_N / \langle \pm 1 \rangle$  is defined as the set of *unsigned* Pauli strings. Then  $C$  is an element of  $\mathcal{U}(2^N)$  is the unitary group of  $N$ -qubit operations, and is defined up to an overall  $\mathcal{U}(1)$  phase.

The action of a Clifford operator  $C \in \mathcal{C}_N$  on a Pauli string  $S_i \in \tilde{\mathcal{P}}_N$  is given by

$$\pm S_{i+1} = C S_i C^\dagger, \quad (2)$$

where  $S_{i+1} \in \tilde{\mathcal{P}}_N$  and the indices  $j = i, i+1, \dots$  label the series of Pauli strings obtained by the action of a Clifford operator. Since the dimension  $|\tilde{\mathcal{P}}_N|$  of the Pauli group is finite, the repeated action of the *same* element  $C$  results in periodic orbits of period  $L$ , defined by the condition

$$C^L S_0 (C^\dagger)^L = \mathbb{C}^L S_0 = \tau S_0, \quad (3)$$

where we introduced the notation  $\mathbb{C}O \equiv C O C^\dagger$  with  $O$  an operator acting on the qubits. On an orbit of length  $L$ , the initial Pauli string  $S_0$  is recovered after  $L$  steps – up to an overall sign  $\tau = \pm 1$ . For any given Clifford operator  $C$ , the number of orbits  $N_C(L, \tau)$  with period  $L$  and parity  $\tau$  fulfills the sum rule

$$\sum_{L, \tau} \tilde{N}_C(L, \tau) = \sum_{L, \tau} L N_C(L, \tau) = |\mathcal{P}_N| = 4^N, \quad (4)$$

where  $\tilde{N}_C(L, \tau)$  denotes the total number of those strings that are on some orbit of length  $L$  and parity  $\tau$ . We can further define the ensemble averaged probability of having

an orbit with period  $L$  and parity  $\tau$  as

$$P(L, \tau) = \langle P_C(L, \tau) \rangle_C, \quad (5)$$

where  $\langle \dots \rangle_C$  denotes the average over Clifford operators. In Fig. 2 (a) we show the probability of Clifford orbits  $P(L) = \sum_{\tau} P(L, \tau)$  for  $N = 16$  qubits. Statistical sampling has been performed over brick-wall Clifford circuits of fixed depth  $D$  as schematically shown in Fig. 1 (without  $T$ -gates at this stage). As stated before, for deep-enough circuits this is equivalent to sample generic  $N$ -qubit Clifford gates  $C \in \mathcal{C}_N$ . The distribution of probabilities  $P(L)$  is denser for short orbits while it is sparser for large orbits, and displays some nontrivial properties. Orbits of length  $L$  come with a large degeneracy. While there are  $4^N$  string configurations, the largest orbit is found to scale only as  $L_{\max} = 2^{N+1}$ . Moreover, the number of *allowed* circuits is exponentially smaller than  $L_{\max}$ . Rather surprisingly, the largest probability is found for  $L = L_{\max}/2$ , and atypically-high probabilities occur at rational multiples of  $L_{\max}$ . Note that as the system size increases, it becomes statistically less likely to sample orbits of length  $L \sim \mathcal{O}(1)$ .

The peculiar distribution of the orbits becomes more apparent by plotting the integrated probability  $I(L/L_{\max})$  for different  $N$ , see Fig. 2(b).  $I(L/L_{\max})$  displays steep jumps at rational multiples of  $L/L_{\max} = p/q$ . The most pronounced jumps occur at  $L/L_{\max} = \{1/2, 1/4, 1/8, 1/16, \dots\}$  but they also appear at fractions  $\{3/8, 5/16, 7/16, \dots\}$ , see Fig. 2(b). With increasing  $N$  the jumps become sharper but their height appears to scale to zero in the thermodynamic limit  $N \rightarrow \infty$ , suggesting that  $I(L/L_{\max})$  may converge to a continuous curve.

The structure of the periodic orbits allows us to establish a connection between the eigenvalue spectrum of Clifford operators  $C$  and  $\mathbb{C}$ . For a given orbit,  $\{S_0, \mathbb{C}S_0, \dots, \mathbb{C}^{L-1}S_0\}$ , we can construct the set of oper-

ators

$$V_m = \sum_{k=0}^{L-1} e^{i\frac{2\pi}{L}km} \mathbb{C}^k S_0, \quad (6)$$

with  $m \in \{0, 1, \dots, L-1\}$  for even parity orbits,  $\tau = 1$ , and  $m \in \{\frac{1}{2}, \dots, L - \frac{1}{2}\}$  for  $\tau = -1$ . Clearly, the  $V_m$ 's are eigenvectors of  $\mathbb{C}$ ,

$$\mathbb{C}V_m = e^{i\Theta_m} V_m \quad \text{with} \quad \Theta_m = \frac{2\pi}{L}m. \quad (7)$$

The eigenvalues of  $\mathbb{C}$  are thus related to the periodic orbits. There are altogether  $4^N$  such eigenvalues, corresponding to the dimension of the space of unsigned Pauli strings.

On the other hand, these eigenvalues (and the phases  $\Theta_m$ ) are also closely related to the  $2^N$  eigenvalues (spectrum) of the Clifford operator  $C$ . In particular, let us denote the eigenvectors and eigenvalues of  $C$  by

$$C|\phi_i\rangle = e^{i\vartheta_i} |\phi_i\rangle. \quad (8)$$

Then  $|\phi_i\rangle\langle\phi_j|$  is an eigenstate of the operator  $\mathbb{C}$  with eigenvalue  $\Theta = \vartheta_i - \vartheta_j$ ,

$$\mathbb{C}|\phi_i\rangle\langle\phi_j| = C|\phi_i\rangle\langle\phi_j|C^\dagger = e^{i(\vartheta_i - \vartheta_j)} |\phi_i\rangle\langle\phi_j|. \quad (9)$$

The structure of the periodic orbits is naturally reflected in the distribution of the corresponding phases  $\theta_j$  on the unit circle. The eigenvalues corresponding to representative periodic orbits of length  $L$  and parity  $\tau$  are shown in Figs. 3(a,b).

Notice that the relation above, relating the spectrum of a unitary operator  $U$  and that of the corresponding operator  $\mathbb{U}$  is general. The spectrum of  $\mathbb{U}$  thus captures spectral correlations in the spectrum of  $U$ . To investigate the properties of the phase distribution, we define the phase correlation function for an ensemble of unitary operators  $U \in \mathcal{U}(2^N)$  as

$$\chi(\vartheta, \vartheta') = \frac{1}{d(d-1)} \sum_{i \neq j=1}^d \langle \delta_{2\pi}(\vartheta - \vartheta_i(U)) \delta_{2\pi}(\vartheta' - \vartheta_j(U)) \rangle_U, \quad (10)$$

where  $\langle \dots \rangle_U$  indicates the statistical average over  $U$ , and  $d = 2^N$  is the dimension of the Hilbert space. Here  $\delta_{2\pi}(\dots)$  denotes the  $2\pi$ -periodic Dirac  $\delta$  function. Notice that we have removed the contribution of the terms with  $i = j$ , and normalized  $\chi(\vartheta, \vartheta')$  as  $\int_0^{2\pi} d\vartheta \int_0^{2\pi} d\vartheta' \chi(\vartheta, \vartheta') = 1$ .

For Haar-random unitaries,  $\chi(\vartheta, \vartheta')$  depends only on the phase difference. To compare spectral correlations in a random Clifford circuit with those in a Haar-random circuit, we therefore introduce the average spectral corre-

lation function as

$$\chi(\Theta) \equiv \int_0^{2\pi} d\vartheta' \chi(\Theta + \vartheta', \vartheta'). \quad (11)$$

Figs. 3(c,d) compare the correlation function of undoped Clifford circuits for different system sizes,  $N$ , revealing the peculiar structure and common features of  $\chi(\Theta)$ . The most prominent peaks are observed at rational multiples of  $\pi$ , including  $\{\pi, 2\pi/3, \pi/2, \pi/3, \pi/4, \pi/8, \dots\}$  which are typically surrounded by regions of lower peak density and intensity. These peaks get contribution from

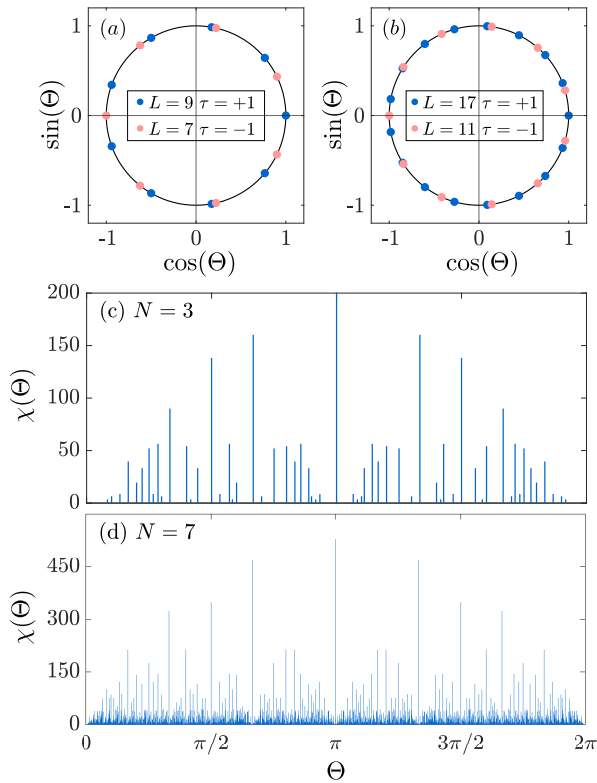


FIG. 3. (a,b) Representative eigenvalue distribution of the Clifford operator  $\mathbb{C}$  on the unit circle, corresponding to orbits of different length  $L$  and parity  $\tau$ . (c,d) Phase correlation function for  $N = 3$  and  $N = 7$  random Clifford circuits. While collecting the data, we used box sizes  $\Delta\Theta = 2\pi/16000$  and  $\Delta\Theta = 2\pi/256000$ . Note the common structure with the highest peaks located at rational multiples of  $\pi$  (see text for a discussion). Histograms were obtained by sampling up to  $N_s = 2^{16}$  circuits.

a large number of orbits. For example, all  $L = \text{even}$  and  $\tau = 1$  orbits as well as all  $L = \text{odd}$  and  $\tau = -1$  orbits have a correlation peak at  $\Theta = \pi$ , while all  $L \equiv 0 \pmod{3}$  orbits with  $\tau = 1$  have a peak at  $\pm 2\pi/3$ . These peaks, especially the peak at  $\Theta = \pi$ , are sensitive indicators of periodic orbits. Although our analysis was not conclusive in this regard, the structure observed is reminiscent of a fractal.

## B. T-doped Clifford circuits

Extending the Clifford group with a single non-Clifford gate (e.g.,  $T$ -gate) is sufficient to achieve universal quantum computing [31, 44, 45]. Hence, the natural goal is to understand how the spectral properties of Clifford circuits change upon *injecting*  $T$ -gates in the random circuit (henceforth Clifford+ $T$  circuits). The expectation is that the circuit properties should converge towards those of Haar distributed operators of the circular unitary ensemble

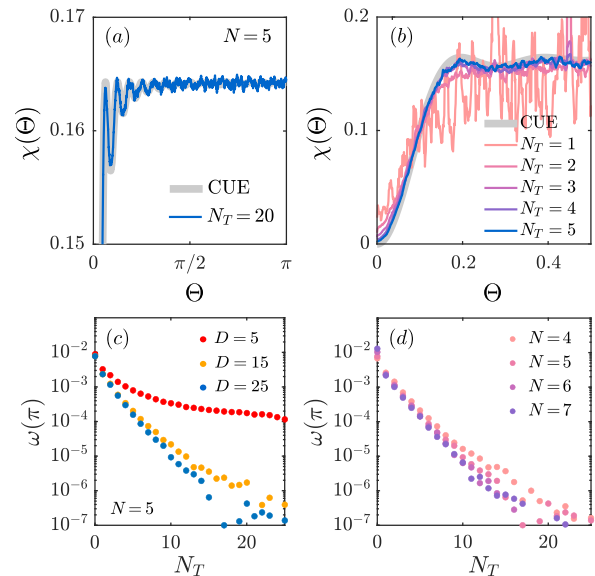


FIG. 4. (a) Comparison of a representative correlation function  $\chi(\Theta)$  for a random Clifford circuit of  $N = 5$  qubits with  $N_T = 20$  injected  $T$ -gates and of depth  $D = 25$  with (blue) against the corresponding analytical result from RMT for the CUE from Eq. (12) (grey). (b) Evolution of  $\chi(\Theta)$  with an increasing number  $N_T$  of  $T$ -gates for a random Clifford circuit of  $N = 5$  qubits, and (c) suppression of the weight  $\omega(\pi)$  of the delta peak at  $\Theta = \pi$  with the number of  $T$ -gates for different values of the circuit depth,  $D = 5$ ,  $D = 15$ , and  $D = 25$ . (d) Suppression of the weight of the  $\Theta = \pi$  peak as a function of  $N_T$  for different values of  $N$  and  $D = 5N$ .

ble (CUE) [46–48]. In this respect, a relevant problem is to quantify *how many*  $T$ -gates are necessary for this convergence. To this end, in the following we consider two quantities: (i) the phase correlation function defined in Eq. (10) and (ii) the level spacing statistics.

### 1. Phase correlation function

The analytic expression for the correlation function of the CUE is known from RMT [47]

$$\chi_{\text{CUE}}(\Theta = \vartheta - \vartheta') = \frac{1}{2\pi} \frac{d}{d-1} \left( 1 - \frac{\sin^2(d\Theta/2)}{d^2 \sin^2(\Theta/2)} \right) \quad (12)$$

For a high number of  $T$ -gates  $N_T \gg 1$ , we find that the correlation function  $\chi(\Theta)$  of a  $T$ -doped Clifford circuits resembles very closely  $\chi_{\text{CUE}}(\Theta)$  as shown in Fig. 4(a), in particular, the characteristic rapid oscillations towards the edge  $\vartheta \sim 0$  are quantitatively reproduced.

Fig. 5 displays the evolution of the correlation function with a few injected  $T$ -gates. The general structure of  $\chi$  is significantly changed already with a *single*  $T$ -gate. Moreover, the characteristic edge features of  $\chi_{\text{CUE}}$  are already recovered *qualitatively* with one  $T$ -gate and *quantitatively* with as few as three  $T$ -gates, cfr. also Fig. 4(b).

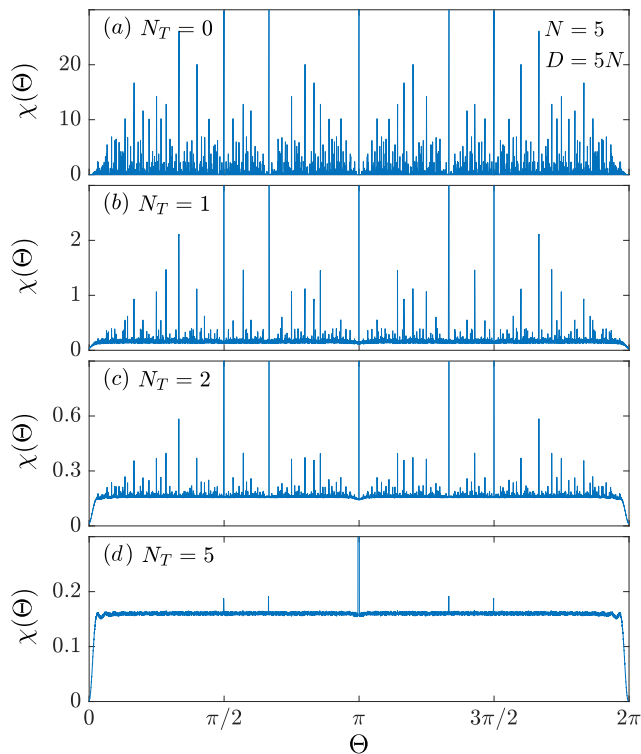


FIG. 5. Evolution of the correlation function for  $N = 5$  qubits with the number of  $T$ -gates  $N_T$ . We used box sizes  $\Delta\Theta = 2\pi/128000$ .

In the central region,  $\Theta \sim \pi$ , the correlation function  $\chi$  is dominated by discrete peaks reminiscent of the structure observed for pure Clifford circuits. These are likely associated with short periodic orbits localized in a portion of the qubit register that statistically survive the effect of a few randomly injected  $T$ -gates. The expectation is that for deep-enough circuits a few  $T$ -gates should scramble most periodic orbits. This is confirmed by the paradigmatic evolution of the feature at  $\Theta = \pi$ , see Fig. 4(c). Notice that already a single  $T$ -gate suppresses exponentially the correlation peak at  $\pi$ , i.e., it removes most periodic orbits, but an exponentially small fraction of periodic orbits seems to survive even in the large  $D$  limit. Also, as a function of  $N_T$ , data for different  $N$ -s appear to collapse to a single curve, suggesting that the fraction of removed periodic orbits depends just on  $N_T$  for deep circuits.

## 2. Level spacing statistics

Another natural measure of how rapidly Clifford+ $T$  circuits converge to the CUE is given by level spacing statistic [49–51]. For any unitary operator  $U \in \mathcal{U}(2^N)$ , we calculate all  $d = 2^N$  eigenvalues of the corresponding Hilbert operator, sort them (so that  $\vartheta_j < \vartheta_k$  for  $j < k$ ), and look at the nearest-neighbor distances  $\zeta \equiv \vartheta_{j+1} - \vartheta_j$ .

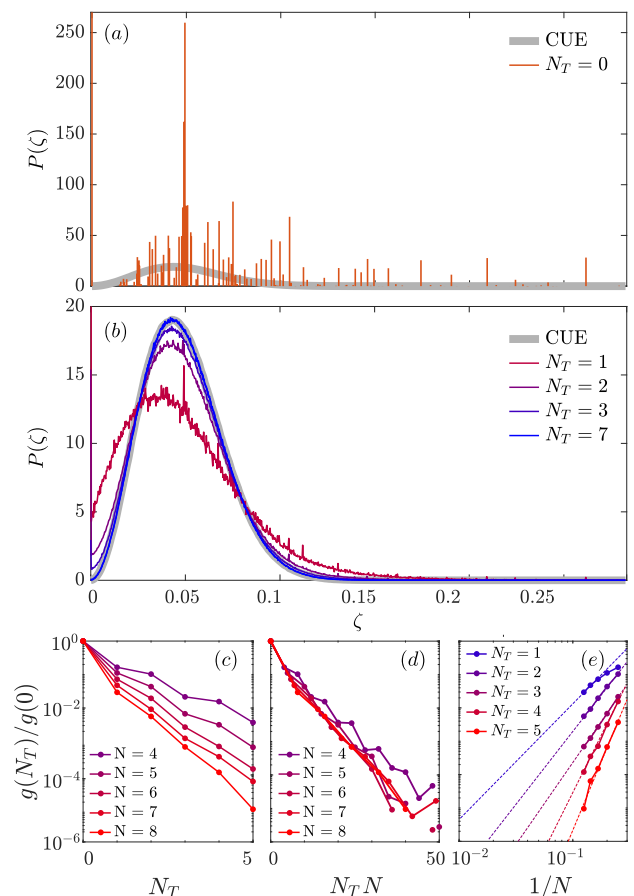


FIG. 6. (a,b) Level spacing distribution of Clifford+ $T$  random circuits (color lines) and Haar random unitaries (gray line) for  $N = 7$  qubits. (a) For pure Clifford circuits ( $N_T = 0$ ) the distribution is characterized by a discrete structure and a high eigenvalue degeneracy, corresponding to the feature at  $\zeta = 0$ . (b) Injecting  $T$ -gates,  $P(\zeta)$  converges to the CUE distribution. (c-e) Fraction of eigenvalue degeneracy  $g(N_T)/g(0)$  for different system sizes  $N$  as a function of  $N_T$  (c), as a function of  $N_T N$  (d), and versus  $1/N$  for different  $N_T$ s (e). The data suggest that in the thermodynamic limit,  $N \rightarrow \infty$ , any finite number of  $T$ -gates eventually resolves all degeneracies (i.e., disrupts all Clifford orbits) for deep-enough circuits. For instance, for  $N_T = 2$ , degeneracies are predicted to be suppressed a million-fold for  $N < 100$  qubits (see dashed line).

Ensemble averaging over  $N_s$  samples yields

$$P(\zeta) = \frac{1}{N_s d} \sum_{i=1}^{N_s} \sum_{j=1}^d \delta_{2\pi}(\zeta - [\vartheta_{j+1}(U_i) - \vartheta_j(U_i)]). \quad (13)$$

We sample both random Clifford+ $T$  circuits and Haar random unitaries to build the corresponding distributions numerically. In Figs. 6(a,b) we compare the level spacing distribution  $P(\zeta)$  for pure Clifford circuits and Haar unitaries. For pure Clifford circuits ( $N_T = 0$ ), the distribution is characterized by a discrete structure and high degeneracies, yielding a delta peak at  $\zeta = 0$ .

Injecting  $T$ -gates, the degeneracies are resolved, and the distribution converges to the CUE result.

Let us now focus on the feature at  $\zeta = 0$ , which corresponds to the fraction of degeneracies  $g(N_T)/g(0)$  (see Fig. 6 (c)). In contrast to the number of periodic orbits, the number of degeneracies is suppressed *faster* with increasing  $N$ , and our data are suggestive of an exponential scaling with  $N \times N_T$ . This is apparently related to the specific structure of periodic orbits. The largest periodic orbit is of size  $L_{\max} \sim 2^N$ , which is exponentially smaller than the number of strings,  $N_{\text{strings}} = 2^{2N}$ . Many of the orbits in undoped Clifford circuits are therefore exponentially large. One can argue that these exponentially large orbits contribute an exponentially large fraction to the degeneracy  $g(0)$ , and, moreover, are exponentially sensitive to the presence of  $T$ -gates, which can destroy them. As a result, the number of degeneracies decreases much faster than the number of periodic orbits, and is suppressed as  $\sim e^{-cN \cdot N_T}$ , while the number of orbits decreases only as  $\sim e^{-c'N_T}$ , with  $c$  and  $c'$  constants of the order of unity. For any finite value of  $N_T$ , the fraction of degeneracies is suppressed as  $N \rightarrow \infty$ . Indeed, the finite size scaling in Fig. 6 (e) suggests that in the limit,  $N \rightarrow \infty$ , any finite number of  $T$ -gates eventually resolves all but a vanishing fraction of degeneracies in the spectrum.

We should add that a periodic orbit  $P$  in the space of strings, as generated by  $U$ , corresponds to a series of eigenphases  $\vartheta = \vartheta_P + 2\pi m/L$  in the spectrum of  $U$ , with  $\vartheta_P \in [0, 2\pi/L]$  a phase associated with the orbit. To have degeneracies in the spectrum of  $U$ , one therefore needs the phases  $\vartheta_P$  of *different* orbits to be correlated. Clearly, in the undoped Clifford circuit this is the case. These observations are also in line with recent results from Haferkamp *et al.* [32], which showed that a *system-independent* number  $\mathcal{O}(k^4 \log_2^2(k) \log_2(1/\epsilon))$  of non-Clifford gates is sufficient to approximate a  $k$ -design with precision  $\epsilon$ .

## IV. MAGIC GENERATION

### A. Stabilizer Rényi Entropy (SRE)

Within quantum resource theory [52], several tools have been proposed to classify quantum resources encoded in a quantum state, as a measure of complexity. Concepts such as entanglement, nonlocality, quantum coherence, quantum correlations, have been investigated within this framework. In this context, the *stabilizer Rényi entropy (SRE)*, also referred to as magic, represents the hardness to classically simulate a quantum state [12, 53], and has raised significant attention recently [17–19, 22, 25, 28, 54, 55].

Within the stabilizer formalism, the *stabilizer states* are reachable from the computational basis states (e.g., from  $|0\rangle^{\otimes N}$ ) using Clifford operations, and can be efficiently represented on a classical computer [5, 6]. By this definition, stabilizer states (elements of STAB) have zero magic. To quantify magic in terms of SRE in a pure state

$|\psi\rangle$ , one first introduces a string probability distribution in the basis of Pauli strings, associated with  $|\psi\rangle$  as

$$\Xi_\psi(S) = \frac{1}{d} \langle \psi | S | \psi \rangle^2, \quad (14)$$

where  $d = 2^N$  is the dimension of the Hilbert space of  $N$  qubits. The corresponding stabilizer 2-Rényi entropy (henceforth simply SRE or magic) associated with this probability distribution reads

$$M_2(|\psi\rangle) = -\log_2 \sum_{S \in \mathcal{P}_N} \Xi_\psi^2(S) - \log_2(d). \quad (15)$$

The SRE also fulfills the following properties [12]:

- (i) *faithfulness*:  $M_2(|\psi\rangle) = 0$  iff  $|\psi\rangle \in \text{STAB}$ , otherwise  $M_2(|\psi\rangle) > 0$ ; stabilizer states thus correspond to states that are relatively localized in the space of strings and have the smallest possible entropy;
- (ii) *stability under Clifford operations*,  $C \in \mathcal{C}_N$ :  $M_2(C|\psi\rangle) = M_2(|\psi\rangle)$ ;
- (iii) *additivity*:  $M_2(|\psi\rangle \otimes |\phi\rangle) = M_2(|\psi\rangle) + M_2(|\phi\rangle)$ ; and
- (iv) it is *upper bounded* by  $M_2(|\psi\rangle) \leq \log_2((d+1)/2)$ .

We remark that for  $N = 1$  and  $N = 3$  qubits, we found states that saturate the upper bound (iv) for the SRE, see Appendix A.

In the context of quantum resource theory, magic is a property of a state. Our goal is, however, to characterize the magic generation properties of an *operator* or, rather, a class of operators, the ensemble of Clifford+ $T$  circuits. A step in this direction has been done with the *nonstabilizing power* of a unitary operator  $U$  [12]

$$\mathcal{M}_2(U) = \frac{1}{|\text{STAB}|} \sum_{|\psi\rangle \in \text{STAB}} M_2(U|\psi\rangle), \quad (16)$$

which associates an average value of SRE to any given unitary operator. This quantity measures the power of a quantum circuit to generate complex states from stabilizer states. For the nonstabilizing power, some interesting results are available [12], including: (i) a lower bound for the typical nonstabilizing power for Haar unitaries  $\langle \mathcal{M}_2(U) \rangle \geq \log_2((d+3)/4)$ , and (ii) a lower bound on the number of  $T$ -gates needed in addition to Clifford circuits to decompose a unitary operator  $U$ , which is found to be  $\gtrsim O(N)$ .

Computing the nonstabilizing power of a quantum circuit  $U$  is very expensive, as it requires evaluating  $M_2$  as in Eq.(15) – which is already a numerically expensive endeavor – and then averaging it over the exponentially large set of stabilizer states, see Eq.(16). Furthermore, in the case of random circuits, an averaging over the ensemble also needs to be performed.

Here we complete this program: we investigate the rate of magic growth in Clifford +  $T$  circuits as a function

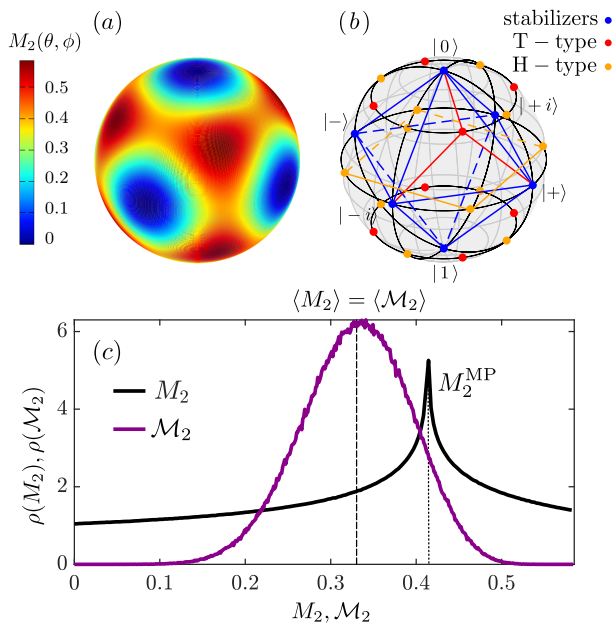


FIG. 7. (a) Color plot of magic on the Bloch sphere for a single qubit. (b) Special states on the Bloch sphere: states with magic  $M_2(|\psi\rangle) = 0$ , i.e., stabilizer states occupy the vertices of an octahedron (blue),  $|0\rangle$ ,  $|1\rangle$ ,  $|+\rangle$ ,  $|-\rangle$ ,  $|+i\rangle$ ,  $| -i\rangle$ ;  $T$ -type states  $|T\rangle$  possess maximal magic,  $M_2 = \log_2(3) - \log_2(2) \approx 0.585$  (red);  $H$ -type states  $|H\rangle$  are associated with the most probable value of magic  $M_2 = M_2^{\text{MP}}$  (orange), see text for a discussion. (c) Distribution of magic,  $\rho(M_2)$ , obtained by sampling 1-qubit states uniformly on the Bloch sphere, and distribution of the nonstabilizing power  $\rho(\mathcal{M}_2)$  of 1-qubit Haar-random unitaries. The two distributions have the same mean value,  $\langle M_2 \rangle_\psi = \langle \mathcal{M}_2 \rangle_U$ , but  $\rho(M_2)$  has a logarithmic singularity at  $M_2^{\text{MP}} \approx 0.414$  corresponding to the  $H$ -type states,  $|H\rangle$ .

of injected  $T$ -gates. We compute numerically the distribution of magic  $\rho(M_2)$  for the ensemble, and compute the average nonstabilizing power  $\langle \mathcal{M}_2 \rangle_U$  as a function of system size,  $N$ , and the number of  $T$ -gates,  $N_T$ .

## B. One Qubit

Before showing the results for more complex Clifford+ $T$  circuits, let us focus on the simplest case of a single qubit, and study the magic of its states, as well as the nonstabilizing power of one-qubit Haar-random gates. While being the simplest instance, analyzing this, provides useful tools to understand the magic generation properties of more complex circuits.

We parametrize 1-qubit states on the Bloch sphere as

$$|\psi\rangle = \cos(\theta/2) |0\rangle + e^{i\varphi} \sin(\theta/2) |1\rangle, \quad (17)$$

and calculate the magic  $M_2(\theta, \varphi)$  on a dense mesh of polar and azimuthal angles,  $0 \leq \theta \leq \pi$ , and  $0 \leq \varphi < 2\pi$ , while weighting with the Haar measure,  $\sim \sin(\theta) d\theta d\varphi$ .

Note that this is equivalent to sampling the unitary operators  $U \in \mathcal{U}(2)$  with uniform Haar measure, and applying  $U$  to the stabilizer state  $|0\rangle$ , or, equivalently, picking states uniformly on the Bloch sphere. We show the magic map on the Bloch sphere in Fig. 7(a), and the corresponding probability density  $\rho(M_2)$  in Fig. 7(c). The maximum achievable magic value we find coincides with the theoretical upper bound [12],  $M_2^{\text{max}} = \log_2((d+1)/2) = \log_2(3/2) = 0.5849\dots$ , proving that the bound is tight for  $N = 1$ .

We identify a few interesting states on the Bloch sphere, as shown in Fig. 7(b). As expected, states with zero magic correspond to the one-qubit stabilizer states  $\{|0\rangle, |1\rangle, |+\rangle, |-\rangle, |i\rangle, |-i\rangle\}$ , which occupy the vertices of an octahedron. Clifford group elements generate symmetry operations on this octahedron [15, 56]. States with maximal SRE,  $M_2^{\text{max}} = 0.585\dots$  are identified as  $T$ -type states (red dots in Fig. 7(b)). A representative  $T$ -type state can be generated as  $THTH|0\rangle$ , where  $H$  denotes the Hadamard gate. The other  $T$ -type states (8 in total) can be obtained from this by applying phase gates  $S$  ( $\pi/2$  rotation), or by combining  $Y$  and  $S$  gates. Another set of interesting states is that of  $H$ -type states (orange dots in Fig. 7(b)), denoted as  $|H\rangle$ . On the magic map in Fig. 7(a), these correspond to saddle points with a magic  $M_2^{\text{MP}} = 0.414\dots$ . This is identified as the most likely magic, associated with the van Hove singularity of the underlying saddle point. A representative  $H$ -state on the equator can be generated as  $TH|0\rangle$ , and all other  $H$ -states (12 in total) can be generated by applying on this state Clifford gates  $H$ ,  $Y$  and  $S$ . Interestingly, these states can be obtained with a protocol known as *magic state distillation*, and allow for universal quantum computing [14, 15, 57, 58].

Finally in Fig. 7(c) we show the one-qubit magic distribution  $\rho(M_2)$ . The distribution is nearly featureless, except for a logarithmic singularity at the most-probable value  $M_2^{\text{MP}}$ , corresponding to the magic of  $H$ -type states. This can be understood as a van Hove singularity due to the saddle point. For comparison, we also show the distribution of the nonstabilizing power  $\rho(\mathcal{M}_2)$  of Haar random single-qubit operators  $U \in \mathcal{U}(2)$ . This we obtained by sampling  $U$ , and calculating the corresponding nonstabilizing power  $\mathcal{M}_2(U)$  from its definition, Eq. (16). The distributions of  $M_2$  and  $\mathcal{M}_2$  display quite different shapes, however, they have the *same* expectation value,  $\langle M_2 \rangle_\psi = \langle \mathcal{M}_2 \rangle_U$ .

## C. Magic generation in Clifford+ $T$ circuits

We investigate magic generation in Clifford+ $T$  circuits [21, 59] by applying the following protocol:

- (i) We initialize the qubit register in a random stabilizer state  $|\psi\rangle = C(|0\rangle^{\otimes N})$ , where  $C$  is a brick-wall Clifford circuit deep enough to represent an element of  $\mathcal{C}_N$ . By construction, this initial state has no magic,  $M_2(|\psi\rangle) = 0$ .



- (ii) Generate a random Clifford+ $T$  circuit  $U$  with a given depth  $D$  and number of injected  $T$ -gates,  $N_T$ .
- (iii) We calculate the magic of this state,  $M_2(U|\psi)$ .
- (iv) We obtain the average nonstabilizing power of the ensemble,  $\langle \mathcal{M}_2 \rangle_U$  by averaging  $M_2(U|\psi)$  over  $N_s = 2^{16}$  initial states and random circuits.

Notice that the procedure above performs a simultaneous average over the stabilizer states as well as the circuit ensemble. Therefore, assuming self-averaging, the average magic of the final states is equal to the average stabilizing power of the circuits,

$$\langle M_2(U|\psi) \rangle_{U,\psi \in \text{STAB}} = \langle \mathcal{M}_2 \rangle_U. \quad (18)$$

This has been explicitly demonstrated in the previous subsection for  $N = 1$ .

Let us note that the numerical evaluation of the magic is exponentially expensive, since the number of (unsigned) Pauli strings  $P \in \mathcal{P}_N$  scales as  $|\mathcal{P}_N| = 4^N$ . It has been shown that the SRE can be computed efficiently for certain classes of states such a matrix product states [19, 20, 23], but not for the general states discussed here. This poses severe limitations to the system sizes investigated within our framework.

As shown in Fig. 8(a), the magic generated by Clifford+ $T$  circuits scales approximately linearly with the number of injected  $T$ -gates in the regime  $N_T \lesssim N$ . While the slope depends on  $N$ , we predict that in the thermodynamic limit,  $N \rightarrow \infty$ , it converges to  $\mathcal{M}_2^\infty(T)$ , i.e., to the nonstabilizing power of a  $T$ -gate applied on a large system of qubits,  $N \gg 1$ . Astonishingly, within our numerical accuracy, the value  $\mathcal{M}_2^\infty(T)$  seems to coincide with the magic of a single qubit  $|H\rangle$ -state,  $\mathcal{M}_2^\infty(T) = M_2^{N=1}(|H\rangle)$ . The reason behind this is that, one the one hand, in large circuits,  $T$ -gates leave only a small fraction of stabilizer states invariant, and transform most of them into  $H$ -like states, and on the other hand, remote  $T$  gates act independently. Therefore, in the sparse  $T$ -gate limit ( $N_T \lesssim N$ ) magic is generated in approximate quanta of size  $M_2^{N=1}(|H\rangle)$ . Magic, however, cannot increase indefinitely: for  $N_T \gtrsim N$  "interference" between multiple  $T$ -gates slows down the magic generation rate, and the average magic, i.e., the average nonstabilizing power of the random circuits,  $\langle \mathcal{M}_2 \rangle$ , saturates. It is natural to expect that the saturation value corresponds to the average of Haar-random unitary circuit nonstabilizing power. This is confirmed by numerical simulations where we averaged over Haar-random unitary circuits, see dashed horizontal line in Figs.8(a,b). This suggest that the typical complexity of a Haar-random circuit can be reached by  $N_T \sim \mathcal{O}(N)$   $T$ -gates.

Another interesting quantity to consider is the nonstabilizing power *density* of Clifford+ $T$  circuits  $\langle \mathcal{M}_2/N \rangle$ . Notice that this coincides with the average *magic density*  $\langle \mathcal{M}_2/N \rangle$  of states generated by the circuit action on stabilizer states. As shown in Fig. 8(b), in the regime with

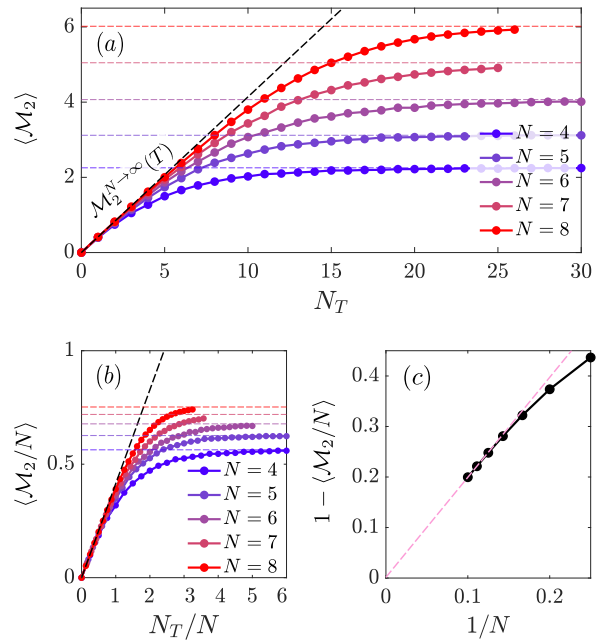


FIG. 8. Magic generation of Clifford+ $T$  circuits for different system sizes  $N$ , and depth  $D = 5N$ . (a) In the sparse limit,  $N_T \lesssim N$ , the average nonstabilizing power scales as  $\langle \mathcal{M}_2 \rangle = \langle \mathcal{M}_2 \rangle \approx \mathcal{M}_2^\infty(T)N_T$ , with  $\mathcal{M}_2^\infty(T) \approx 0.414$  the average nonstabilizing power of a single  $T$ -gate acting on a system of  $N \rightarrow \infty$  qubits. Horizontal dashed lines denote the average nonstabilizing power computed for Haar random unitaries. (b) The average non-stabilizing power density  $\langle \mathcal{M}_2/N \rangle$  as a function of  $N_T/N$ . In the limit of  $N_T \lesssim N$  displays a universal slope. In the limit  $N_T \gg N$ , it recovers the value calculated for Haar-random unitaries (dashed lines). (c) Asymptotic values of  $\langle \mathcal{M}_2/N \rangle$ , as computed for Haar-random unitaries, plotted against  $1/N$ .

only a few injected  $T$ -gates ( $n_T = N_T/N \lesssim 1$ ), the curves display a universal slope:

$$\langle \mathcal{M}_2/N \rangle \approx \mathcal{M}_2^\infty(T) n_T. \quad (19)$$

Finally, in Fig. 9 we discuss the evolution of the probability distribution of the normalized or *magic density*,  $\mu \equiv \mathcal{M}_2/N$ . We have sampled the probability density  $\rho(\mu)$  numerically for different numbers of randomly positioned  $T$ -gates,  $N_T$ , while acting on stabilizer states with Clifford+ $T$  circuits. In the case of a single  $T$ -gate,  $N_T = 1$ , we find that the distribution is *discrete* and *bimodal*, and the only two possible normalized SRE values are  $\mu = 0$  and,  $\mu_H$ , corresponding to the magic of a single qubit  $H$ -type states. As  $N_T$  increases, the spectrum of magic values increases exponentially. Among those, we find (approximate) integer multiples of  $\mu_H$  as well as intermediate values. Eventually, for an *extensive* number of injected  $T$ -gates, the magic displays a quasi-continuous spectrum, but low-magic values are statistically unlikely (see Fig. 9(a)). The corresponding distribution  $\rho(\mu)$  be-

comes skewed and peaked at higher values, which nevertheless remain significantly below the theoretical upper bound for  $N = 6$ .

For the brick-wall Clifford+ $T$  circuits with a finite depth, there exists a *fully-saturated* limit, corresponding to  $N_T = ND$  injected  $T$ -gates. In that limit, we find that  $\rho(\mu)$  approaches to the corresponding magic distribution of states generated by Haar random unitaries, with an accuracy threshold limited by statistical noise due to sampling.

The typical value of the Haar SRE distribution respects the predicted *lower* bound for the typical the nonstabilizing power  $\mathbb{E}_U[\mathcal{M}_2(U)] \geq \log_2((d+3)/4)$  [12]. In particular,  $\langle \mu \rangle \geq \log_2((d+3)/4)/N = 0.677\dots$  for  $N = 6$ . Notice that this lower bound approaches unity as  $1 - 2/N$ , in the thermodynamic limit,  $N \rightarrow \infty$ . Therefore we conjecture, that in the thermodynamic, limit the nonstabilizing power of a deep random  $T$ -doped Clifford circuit becomes

$$\langle \mathcal{M}_2/N \rangle_{N \rightarrow \infty} = \begin{cases} \mathcal{M}_2^\infty(T) n_T & \text{for } n_T < n_T^*, \\ 1 & \text{for } n_T > n_T^*, \end{cases} \quad (20)$$

with  $n_T^* = 1/\mathcal{M}_2^\infty \approx 2.41$ .

As mentioned before, however, for the relatively small number of qubits considered here finite size corrections are large. This is demonstrated in Fig.8 (c), where we display  $1 - \langle \mu \rangle$  as a function of  $1/N$ , as computed for Haar-random circuits. Our data are clearly consistent with a slow,  $\sim 1/N$  convergence,  $\langle \mu \rangle \rightarrow 1$ .

## V. CONCLUSIONS AND OUTLOOK

In this work, we examined how complexity is reflected in the spectral properties and magic generation capabilities of random  $T$ -gate-doped Clifford circuits. For pure Clifford circuits,  $\mathcal{C}$ , we uncovered a unique periodic orbit structure in the space of Pauli strings, which gives rise to large degeneracies in the spectrum as well as delta-correlations. These properties reflect the inherent simplicity of Clifford circuits, which, despite their capacity to generate entanglement, remain efficiently simulable due to their lack of nonstabilizerness or "magic." At the same time, these spectral features turn out to be sensitive indicators of (non)-complexity; they capture accurately how periodic orbits and corresponding spectral degeneracies are destroyed upon  $T$ -doping.

For a finite number of  $T$ -gates,  $N_T$ , and a finite number of qubits,  $N$ , spectral correlations as well as level spacing statistics reveal the simultaneous development of chaotic features described by random-matrix theory, coexisting with exponentially suppressed Clifford-anomalies. For the deep circuits studied here,  $D \gg N$ , the number of periodic orbits is reduced with the number of  $T$ -gates as  $e^{-c N_T}$ , while the degeneracy anomaly in the level spacing distribution, is suppressed roughly as  $e^{-c' N_T N}$ . Therefore, in the thermodynamic limit, even a single  $T$ -

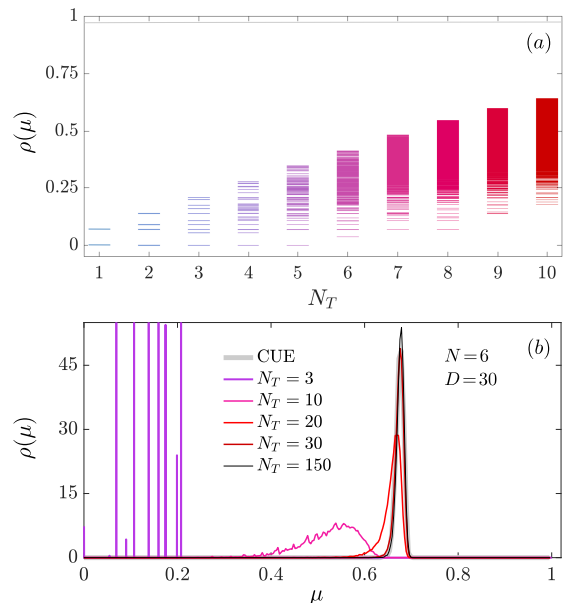


FIG. 9. Evolution of the magic distribution in Clifford+ $T$  circuits for  $N = 6$  qubits and  $D = 5N$ . (a) Spectrum of the normalized SRE as a function of  $N_T$  (lines from blue to red). For a few injected  $T$ -gates the spectrum is discrete, but eventually becomes quasi-continuous as  $N_T$  increases. (b) Magic density distribution  $\rho(\mu)$  for selected values of  $N_T$ . The limiting distribution, i.e., for fully-saturated circuits with  $N_T \rightarrow DN$ , converges to the numerically sampled distribution for Haar unitaries (CUE). For  $N = 6$ , most of the weight is found in a sharp peak at a value that is well below the theoretical maximum.

gate is sufficient to drive the entire spectrum of the circuit towards chaotic behavior, as captured by RMT.

We have also investigated the emergence of complexity in terms of magic generation – referred to as stabilizer Renyi entropy (SRE) [12]. The complexity or nonCliffordness of a given quantum circuit,  $U$ , can be characterized by the average magic generated by that circuit from non-magic (non-complex) stabilizer states. The corresponding quantity, the *nonstabilizing power*, which we could refer to as the *magicness of the circuit*, characterizes the complexity of the quantum circuit. In particular, classically simulatable Clifford circuits have vanishing nonstabilizing power.

Here we investigated, how introducing  $T$ -gates to Clifford circuits impacts the distribution of magic in the final states, and the (average) nonstabilizing power of the circuits. In the dilute limit,  $N_T \ll N$ , the interplay between  $T$ -gates is statistically irrelevant, and the magic generation properties can be entirely understood in terms of the magic generated by a single  $T$ -gate on typical stabilizer states,  $\mathcal{M}_2^\infty(T) = 0.414\dots$ . We find that the average magic – and thus the average stabilizing power of a circuit – increases as  $\langle \mathcal{M}_2 \rangle \approx \mathcal{M}_2^\infty(T) N_T$  for  $N_T \ll N$ . The average magic and the average nonstabilizing power of a circuit  $\langle \mathcal{M}_2 \rangle$  saturates at  $N_T \gtrsim N$ , where

it converges to the nonstabilizing power of Haar-random unitaries. Remarkably, the latter is bounded from below as  $\langle M_2 \rangle_{\text{Haar}} \geq \log_2((d+3)/4) = N - 2 + \dots$  [12]. Therefore, in the  $N \rightarrow \infty$  limit, the saturation value of the average nonstabilizing power density of the circuits – also equal to the average magic density of the final state – behaves as  $\langle \mu \rangle = \langle M_2/N \rangle = 1 - 2/N + \dots$ , and converges to  $\langle \mu \rangle \rightarrow 1$ . Our data indicate furthermore that this property also holds above a critical  $T$ -gate density,  $n_T^* = 1/\mathcal{M}_2^\infty \approx 2.41$ , beyond which magic density *always* converges to its maximal value,  $\mu = 1$ , as  $N \rightarrow \infty$ . We must also add that with increasing  $N$ , the probability density of magic becomes sharper and sharper, and in the thermodynamic limit,  $N \rightarrow \infty$ , the magic density  $\mu$  as well as the nonstabilizing power density become deterministic functions of the  $T$ -gate density,  $n_T = N_T/N$ . Our numerics as well as our analytical arguments show that the thermodynamic relation,  $\mu = \mu(n_T)$  is particularly simple:  $\mu = \lim_{N \rightarrow \infty} \langle \mu \rangle = 1$  for  $n_T > n_T^*$ , while  $\mu$  just scales linearly with  $n_T$  for  $n_T < n_T^*$ ,

$$\mu = \mathcal{M}_2^\infty(T) \cdot n_T \quad \text{if } n_T < n_T^*. \quad (21)$$

This feature is indicative that, in general, around  $N_T \approx 2.41 N$  number of  $T$ -gates are needed in a deep Clifford circuit to generate the complexity of typical Haar random circuits. We should add that for  $N \rightarrow \infty$  this determines the nonstabilizing power of a *typical* random Clifford+ $T$  circuit, too.

Finally, let us comment on the magic (SRE) spectrum of Clifford+ $T$ -gates, when applied on stabilizer states. Upon injecting  $T$ -gates in the circuit, the SRE spectrum evolves from a discrete to a quasi-continuous spectrum, with a distribution generally skewed towards higher values. For high  $T$ -gate doping the distribution becomes strongly peaked, and converges to the distribution of Haar random unitaries.

These findings highlight the interplay between simplicity and complexity in quantum circuits, providing an understanding of how adding non-Clifford elements induces chaotic and resource-rich behaviors. They indicate further that generic unitary operations may be approximated by Clifford+ $T$  circuits with an extensive but still limited number  $N_T \sim N$  of  $T$ -gates.

## ACKNOWLEDGMENTS

We thank A. Hamma for insightful discussions. This research was supported by the Ministry of Culture and Innovation and the National Research, Development and Innovation Office (NKFIH) within the Quantum Information National Laboratory of Hungary (Grant No. 2022-2.1.1-NL-2022-00004), through NKFIH research grants

Nos. K134983, SNN139581, and QuantERA ‘QuSiED’ grant No. 101017733. D.S. acknowledges the professional support of the doctoral student scholarship program of the co-operative doctoral program of the Ministry for Innovation and Technology from the source of the National Research, Development and Innovation fund. C.P.M. acknowledges support by the Ministry of Research, Innovation and Digitization, CNCS/CCCDI-UEFISCDI, under the project PN-IV-P1-PCE-2023-0159. T.R. was supported by the HUN-REN Welcome Home and Foreign Researcher Recruitment Programme 2023.

## Appendix A: Maximum magic states

The theoretical upper bound of the SRE was determined by maximizing the sum corresponding to the projection of state  $|\psi\rangle$  on the  $N$ -qubit Pauli basis, with weights  $\Xi_I = d^{-1}$  and  $\Xi_{P \in \mathcal{P}_N/I} = d^{-1}(d+1)^{-1}$  [12]. We identified states that satisfy these criteria for  $N = 1$  and  $N = 3$  qubits, while demonstrating that these criteria cannot be satisfied for  $N = 2$  qubits.

For a single qubit, the maximum magic state can be found by writing down the equations for the SRE for a generic  $\Xi_P$  and solve it for the criterion above. From symmetry considerations, it immediately follows that the state with maximum magic  $M_2 = \log_2(3/2)$  takes the form

$$|\psi\rangle = \frac{1}{\sqrt{2}} \left( |0\rangle + e^{i\pi/4} |1\rangle \right) = |T\rangle, \quad (A1)$$

which corresponds to one of the 8 T-type states on the Bloch sphere, as shown in Fig. 7(b).

For  $N = 2$ , our analysis of the system of equations yields contradicting constraints. Hence, a state that possess the theoretical upper bound magic  $M_2 = \log_2(5/2)$  does not exist.

For  $N = 3$  qubits we have employed a combinations of Monte Carlo and variational approaches. These led us to a set of states of simple structure

$$|\psi\rangle = \mathcal{N} \sum_j c_j |j\rangle, \quad (A2)$$

where  $c_j \in \{1, i, 1+i, 0\}$ , and  $\mathcal{N}$  is the appropriate normalization. We have identified 448 such states for  $N = 3$  which possess magic  $M_2 = \log_2(9/2)$ . A representative state of this set takes the form

$$|\psi\rangle = \frac{1}{\sqrt{6}} (|000\rangle + |001\rangle + |010\rangle + i|011\rangle + (1+i)|100\rangle). \quad (A3)$$

[1] G. Jaeger, *Classical and quantum computing* (Springer, 2007).

[2] E. Chitambar and G. Gour, Quantum resource theories,

- Reviews of modern physics **91**, 025001 (2019).
- [3] R. Jozsa and N. Linden, On the role of entanglement in quantum-computational speed-up, Proceedings of the Royal Society of London. Series A: Mathematical, Physical and Engineering Sciences **459**, 2011 (2003).
- [4] G. Vidal, Efficient classical simulation of slightly entangled quantum computations, Physical review letters **91**, 147902 (2003).
- [5] D. Gottesman, Theory of fault-tolerant quantum computation, *Physical Review A* **57**, 127–137 (1998).
- [6] S. Aaronson and D. Gottesman, Improved simulation of stabilizer circuits, Physical Review A—Atomic, Molecular, and Optical Physics **70**, 052328 (2004).
- [7] A. Nahum, J. Ruhman, S. Vijay, and J. Haah, Quantum entanglement growth under random unitary dynamics, Physical Review X **7**, 031016 (2017).
- [8] H. Kim and D. A. Huse, Ballistic spreading of entanglement in a diffusive nonintegrable system, Physical review letters **111**, 127205 (2013).
- [9] A. Chandran and C. Laumann, Semiclassical limit for the many-body localization transition, Physical Review B **92**, 024301 (2015).
- [10] M. Žnidarič, Entanglement growth in diffusive systems, Communications Physics **3**, 100 (2020).
- [11] C. W. von Keyserlingk, T. Rakovszky, F. Pollmann, and S. L. Sondhi, Operator hydrodynamics, otocs, and entanglement growth in systems without conservation laws, Physical Review X **8**, 021013 (2018).
- [12] L. Leone, S. F. Oliviero, and A. Hamma, Stabilizer rényi entropy, Physical Review Letters **128**, [10.1103/physrevlett.128.050402](https://doi.org/10.1103/physrevlett.128.050402) (2022).
- [13] V. Veitch, S. H. Mousavian, D. Gottesman, and J. Emerson, The resource theory of stabilizer quantum computation, New Journal of Physics **16**, 013009 (2014).
- [14] S. Bravyi and A. Kitaev, Universal quantum computation with ideal clifford gates and noisy ancillas, Physical Review A **71**, [10.1103/physreva.71.022316](https://doi.org/10.1103/physreva.71.022316) (2005).
- [15] H. Anwar, E. T. Campbell, and D. E. Browne, Qutrit magic state distillation, *New Journal of Physics* **14**, 063006 (2012).
- [16] D. Litinski, Magic state distillation: Not as costly as you think, *Quantum* **3**, 205 (2019).
- [17] S. F. E. Oliviero, L. Leone, A. Hamma, and S. Lloyd, Measuring magic on a quantum processor, npj Quantum Information **8**, [10.1038/s41534-022-00666-5](https://doi.org/10.1038/s41534-022-00666-5) (2022).
- [18] D. Rattacaso, L. Leone, S. F. E. Oliviero, and A. Hamma, Stabilizer entropy dynamics after a quantum quench, Physical Review A **108**, [10.1103/physreva.108.042407](https://doi.org/10.1103/physreva.108.042407) (2023).
- [19] T. Haug and L. Piroli, Quantifying nonstabilizerness of matrix product states, Physical Review B **107**, [10.1103/physrevb.107.035148](https://doi.org/10.1103/physrevb.107.035148) (2023).
- [20] G. Lami and M. Collura, Nonstabilizerness via perfect pauli sampling of matrix product states, Physical Review Letters **131**, [10.1103/physrevlett.131.180401](https://doi.org/10.1103/physrevlett.131.180401) (2023).
- [21] M. Bejan, C. McLauchlan, and B. Béri, Dynamical magic transitions in monitored clifford+t circuits, PRX Quantum **5**, [10.1103/prxquantum.5.030332](https://doi.org/10.1103/prxquantum.5.030332) (2024).
- [22] T. Haug, S. Lee, and M. Kim, Efficient quantum algorithms for stabilizer entropies, Physical Review Letters **132**, [10.1103/physrevlett.132.240602](https://doi.org/10.1103/physrevlett.132.240602) (2024).
- [23] P. S. Tarabunga, E. Tirrito, M. C. Bañuls, and M. Dalmonte, Nonstabilizerness via matrix product states in the pauli basis, Physical Review Letters **133**, [10.1103/physrevlett.133.010601](https://doi.org/10.1103/physrevlett.133.010601) (2024).
- [24] P. Niroula, C. D. White, Q. Wang, S. Johri, D. Zhu, C. Monroe, C. Noel, and M. J. Gullans, Phase transition in magic with random quantum circuits, *Nature Physics* **20**, 1786–1792 (2024).
- [25] X. Turkishi, Coherent errors make magic, *Nature Physics* **20**, 1696–1697 (2024).
- [26] C. Gidney, N. Shutty, and C. Jones, Magic state cultivation: growing t states as cheap as cnot gates, arXiv preprint arXiv:2409.17595 (2024).
- [27] G. E. Fux, B. Béri, R. Fazio, and E. Tirrito, *Disentangling unitary dynamics with classically simulable quantum circuits* (2024).
- [28] X. Turkishi, E. Tirrito, and P. Sierant, *Magic spreading in random quantum circuits* (2024).
- [29] A. Y. Kitaev, Quantum computations: algorithms and error correction, *Russian Mathematical Surveys* **52**, 1191–1249 (1997).
- [30] D. Litinski, A game of surface codes: Large-scale quantum computing with lattice surgery, *Quantum* **3**, 128 (2019).
- [31] S. Bravyi and D. Gosset, Improved classical simulation of quantum circuits dominated by clifford gates, Physical review letters **116**, 250501 (2016).
- [32] J. Haferkamp, F. Montealegre-Mora, M. Heinrich, J. Eisert, D. Gross, and I. Roth, Efficient unitary designs with a system-size independent number of non-clifford gates, *Communications in Mathematical Physics* **397**, 995–1041 (2022).
- [33] S. Zhou, Z. Yang, A. Hamma, and C. Chamon, Single t gate in a clifford circuit drives transition to universal entanglement spectrum statistics, *SciPost Physics* **9**, [10.21468/scipostphys.9.6.087](https://doi.org/10.21468/scipostphys.9.6.087) (2020).
- [34] J. Pöschel, A lecture on the classical kam theorem, arXiv preprint arXiv:0908.2234 (2009).
- [35] Y. Wang and Y. Li, Stabilizer rényi entropy on qudits, *Quantum Information Processing* **22**, 444 (2023).
- [36] T. Haug and L. Piroli, Stabilizer entropies and nonstabilizerness monotones, *Quantum* **7**, 1092 (2023).
- [37] C. Vairogs and B. Yan, Extracting randomness from quantum magic, arXiv preprint arXiv:2402.10181 (2024).
- [38] Y. Zhang and Y. Gu, Quantum magic dynamics in random circuits, arXiv preprint arXiv:2410.21128 (2024).
- [39] S. Zhou, Z.-C. Yang, A. Hamma, and C. Chamon, Single T gate in a Clifford circuit drives transition to universal entanglement spectrum statistics, *SciPost Phys.* **9**, 087 (2020).
- [40] M. Mezei and D. Stanford, On entanglement spreading in chaotic systems, *Journal of High Energy Physics* **2017**, 1 (2017).
- [41] C. W. von Keyserlingk, T. Rakovszky, F. Pollmann, and S. L. Sondhi, Operator hydrodynamics, otocs, and entanglement growth in systems without conservation laws, Physical Review X **8**, 021013 (2018).
- [42] S. Bravyi and D. Maslov, Hadamard-free circuits expose the structure of the clifford group, *IEEE Transactions on Information Theory* **67**, 4546–4563 (2021).
- [43] E. Van Den Berg, A simple method for sampling random clifford operators, in *2021 IEEE International Conference on Quantum Computing and Engineering (QCE)*, Vol. 8 (IEEE, 2021) p. 54–59.
- [44] S. Bravyi and A. Kitaev, Universal quantum computation with ideal clifford gates and noisy ancillas, Physical Review A—Atomic, Molecular, and Optical Physics **71**, 022316 (2005).

- [45] M. Hinsche, M. Ioannou, A. Nietner, J. Haferkamp, Y. Quek, D. Hangleiter, J.-P. Seifert, J. Eisert, and R. Sweke, One t gate makes distribution learning hard, *Physical Review Letters* **130**, 240602 (2023).
- [46] P. Deift and D. Gioev, *Random matrix theory: invariant ensembles and universality*, Vol. 18 (American Mathematical Soc., 2009).
- [47] H. Gharibyan, M. Hanada, S. H. Shenker, and M. Tezuka, Onset of random matrix behavior in scrambling systems, *Journal of High Energy Physics* **2018**, 1 (2018).
- [48] P. J. Forrester, A review of exact results for fluctuation formulas in random matrix theory, *Probability Surveys* **20**, 170 (2023).
- [49] M. Carmeli, Statistical theory of energy levels and random matrices in physics, *Journal of Statistical Physics* **10**, 259 (1974).
- [50] K. Życzkowski and M. Kus, Random unitary matrices, *Journal of Physics A: Mathematical and General* **27**, 4235 (1994).
- [51] S. True and A. Hamma, Transitions in entanglement complexity in random circuits, *Quantum* **6**, 818 (2022).
- [52] E. Chitambar and G. Gour, Quantum resource theories, *Reviews of Modern Physics* **91**, 10.1103/revmod-phys.91.025001 (2019).
- [53] J. Huang, X. Qian, and M. Qin, Non-stabilizerness entanglement entropy: a measure of hardness in the classical simulation of quantum many-body systems (2024).
- [54] L. Leone and L. Bittel, Stabilizer entropies are monotones for magic-state resource theory, *Physical Review A* **110**, 10.1103/physreva.110.1040403 (2024).
- [55] A. Ahmadi and E. Greplova, Quantifying non-stabilizerness via information scrambling, *SciPost Physics* **16**, 10.21468/scipostphys.16.2.043 (2024).
- [56] S. Virmani, S. F. Huelga, and M. B. Plenio, Classical simulability, entanglement breaking, and quantum computation thresholds, *Physical Review A* **71**, 10.1103/physreva.71.042328 (2005).
- [57] A. Krishna and J.-P. Tillich, Towards low overhead magic state distillation, *Physical review letters* **123**, 070507 (2019).
- [58] N. Bao, C. Cao, and V. P. Su, Magic state distillation from entangled states, *Physical Review A* **105**, 022602 (2022).
- [59] X. Li and S. Luo, Optimality of t-gate for generating magic resource, *Communications in Theoretical Physics* **75**, 045101 (2023).